Atmos. Chem. Phys. Discuss., 12, 14197–14246, 2012
www.atmos-chem-phys-discuss.net/12/14197/2012/
doi:10.5194/acpd-12-14197-2012

Atmospheric Chemistry and Physics Discussions

Aerosol indirect effect on warm clouds over South-East Atlantic, from co-located MODIS and CALIPSO observations

L. Costantino and F.-M. Bréon

Laboratoire des Sciences du Climat et de l'Environnement, Unité Mixte de Recherche, CEA-CNRS-UVSQ, 91191 Gif sur Yvette, France

Received: 25 April 2012 – Accepted: 15 May 2012 – Published: 7 June 2012

Correspondence to: L. Costantino (lore.costantino@gmail.com)

Published by Copernicus Publications on behalf of the European Geosciences Union.

Abstract

In this study, we provide a comprehensive analysis of aerosol interaction with warm boundary layer clouds, over South-East Atlantic. We use MODIS retrievals to derive statistical relationships between aerosol concentration and cloud properties, together with co-located CALIPSO estimates of cloud and aerosol layer altitudes. The latter are used to differentiate between cases of mixed and interacting cloud-aerosol layers from cases where the aerosol is located well-above the cloud top. This strategy allows, to a certain extent, to isolate real aerosol-induced effect from meteorology.

Similar to previous studies, statistics clearly show that aerosol affects cloud microphysics, decreasing the Cloud Droplet Radius (CDR). The same data indicate a concomitant strong decrease in cloud Liquid Water Path (LWP), in evident contrast with the hypothesis of aerosol inhibition of precipitation (Albrecht, 1989). Because of this water loss, probably due to the entrainment of dry air at cloud top, Cloud Optical Thickness (COT) is found to be almost insensitive to changes in aerosol concentration. The analysis of MODIS-CALIPSO coincidences also evidenced an aerosol enhancement of low cloud cover. Surprising, the Cloud Fraction (CLF) response to aerosol invigoration is much stronger when (absorbing) particles are located above cloud top, than in cases of physical interaction, This result suggests a relevant aerosol radiative effect on low cloud occurrence. Heating the atmosphere above the inversion, absorbing particles above cloud top may decrease the vertical temperature gradient, increase the low tropospheric stability and provide favorable conditions for low cloud formation.

We also focus on the impact of anthropogenic aerosols on precipitation, through the statistical analysis of CDR-COT co-variations. A COT value of 10 is found to be the threshold beyond which precipitation mostly forms, in both clean and polluted environments. For larger COT, polluted clouds showed evidence of precipitation suppression. Results suggest the presence of two competing mechanisms governing LWP response to aerosol invigoration: a drying effect due to aerosol enhanced entrainment of dry air at

ACPD

12, 14197–14246, 2012

cloud top (predominant for optically thin clouds) and a moistening effect due to aerosol inhibition of precipitation (predominant for optically thick clouds).

1 Introduction

The importance of anthropogenic aerosol impact on cloud has been documented by the Intergovernmental Panel on Climate Change (IPCC) 2007, which also stresses the large uncertainties both in the competing processes and the quantification of their impact. An increase in particle concentration acting as CCN (Cloud Condensation Nuclei) can enhance Cloud Droplet Number Concentration (CDNC), resulting in a reduction of mean droplet size (Bréon et al., 2002). For the same spatial distribution of liquid water, a cloud made of more numerous small droplets, reflects more than a cloud with fewer and larger droplets (Twomey, 1974, 1977). Thus, an increase in aerosol load can lead to an increase in cloud reflectance, if cloud water amount remains constant. This process, known with the name of "Twomey's effect" or "first Aerosol Indirect Effect" (AIE #1), can produce a negative forcing on Earth radiative balance, with a net cooling effect on climate. In addition, a strong feedback to AIE #1 may rise from the higher concentration of droplets with smaller Cloud Droplet effective Radius (CDR) in polluted clouds, where collision-coalescence processes can be suppressed and precipitation efficiency decreased (Albrecht, 1989). Inhibition of precipitation may lead to increased cloud lifetime and cloud Liquid Water Path (LWP), with a possible further increase in Cloud Optical Thickness (COT) and cloud reflectance. This process, known as "second aerosol indirect effect" (AIE #2), would ultimately modify cloud cover in a way that is still poorly quantified.

Aerosol impact on cloud microphysics (cloud droplet concentration and size distribution) has been studied since the late 50's. Warner and Twomey (1967) and Warner (1967) reported of an increase of CCN number concentration, as consequence of the incorporation into clouds of smoke aerosol from sugar cane fires, with decrease of cloud droplet mean radius (potentially impeding the growth of rain drops for coales-

ACPD
12, 14197–14246, 2012

cence). At present days, aerosol impact on cloud microphysics has been well established on global scale by numerous satellite-based analysis (e.g. Bréon et al., 2002; Feingold et al., 2003; Costantino and Bréon, 2010). However, the liquid water path response is far from being well understood. A number of studies show a significant positive correlation between liquid water path and CCN (Quaas et al., 2008; Loeb and Shuster, 2008; Quaas et al., 2009), some others a small but positive correlation (Nakajima et al., 2001; Sekiguchi et al., 2003), some others a negative correlation (Twohy et al., 2005; Matsui et al., 2006; Lee at al., 2009) while others affirm that this relationship can be positive or negative (Han et al., 2002), depending on cloud regime (Lebsock, 2008), on the humidity profile above cloud top (Ackerman et al., 2004), or be mostly driven by local meteorology (Menon et al., 2008). In conclusions, the ultimate aerosol effect on COT and cloud albedo remains still uncertain, leading to strong uncertainties in the quantification of aerosol indirect radiative forcing.

For what concerns the aerosol impact on cloud life cycle, a strong positive relationship between Cloud Fraction (CLF) and Aerosol Optical Depth (AOD) is generally found in several satellite-based analysis (Menon et al., 2008; Quaas et al., 2009; Quaas et al., 2010). Many studies (reviewed by Stevens and Feingold, 2009) agree on the fact that aerosol optical depth and low cloud incidence correlate well with the same meteorological parameters (surface wind speed, atmospheric moisture and stability, etc.). Local variations of one of these parameters can result in apparent correlations between aerosol and cloud retrievals. Therefore, one of the first and most difficult issues of present time research is to separate the impact of meteorology from aerosol-induced effects. Artifact from satellite retrieval errors can also affect statistics, as in case of the cloud adjacent effect (Marshak et al., 2008; Wen et al., 2008; Varnai and Marshak, 2009) and cloud contamination (Kaufman et al., 2005b).

1.1 Purpose and Strategy

The ultimate goal of present work is to use satellite remote sensing observation from simultaneous MODIS and CALIPSO retrievals of aerosol and cloud properties to pro-

ACPD
12, 14197–14246, 2012

vide further experimental evidence of aerosol-induced effect on microphysics (CDR), optical properties (COT), structure (LWP, CLF) and life cycle (precipitation occurrence) of warm boundary layers clouds over South-East Atlantic, quantifying the strength of the interaction.

The main idea is to use CALIPSO data to derive the respective position of cloud and aerosol layers which drives whether they are in direct (other than radiative) interaction. For a given spatial location, if aerosol and cloud layers overlap or their altitudes are very close (within a certain threshold) they are considered interacting. In that case, a change in cloud properties with respect to a variation in aerosol concentration is interpreted as an aerosol driven process. On the other hand, if aerosol and cloud layers are well separated, the observed cloud change is considered as induced by other causes than cloud-aerosol interaction. Even if the deficiency of temporal resolution does not allow to fully assess causality from statistics, the analysis of MODIS-CALIPSO coincidences provide a unique possibility to isolate (to a certain degree) aerosol-induced effects from meteorology and obtain more reliable estimates of aerosol impact on clouds, than simple relationships only based on vertically integrated measurements.

South-East Atlantic region is particularly suited to investigate aerosol indirect effects. Large amount of aerosol load, produced from fires in Southern Africa occurring annually (Ichoku et al., 2003; Edwards et al., 2006), are injected into the atmosphere and transported by trade winds over the Atlantic ocean (Labonne et Bréon, 2007), where a semi-permanent low cloud field is present. In the absence of wet scavenging, the aerosol layers can stay suspended in the atmosphere for days and be transported to considerable distances. South-East Atlantic is one specific area where large aerosol loads are transported above the cloud deck, well separated from it. Aerosol released from savanna and cropland fires mostly contains Organic Carbon (OC) with various amounts of Black Carbon (BC, emitted primarily in efficient flaming fires), depending on the particular fuel, oxygen availability and combustion phase (Andreae and Merlet, 2001). As a consequence of its strong absorption properties, the aerosol layer may warm the atmosphere above the cloud field. Because the underlying surface is bright

ACPD
12, 14197–14246, 2012

and reflects to space a large fraction of the incoming solar radiation in the absence of aerosols, the atmospheric absorption results in a net positive forcing at the Top Of the Atmosphere (TOA). In case of cloud and aerosol mixing, smoke particles can be activated as CCN (because of their relatively high solubility). The effect of their physical interaction with water droplets can be statistically quantified by long term satellite observations.

In this context, our objective is to attempt a quantification of the various aerosol-cloud interaction processes over the South-East Atlantic, where very specific conditions prevail.

1.2 Theoretical background

1.2.1 Cloud optical properties

The first aerosol indirect effect can be quantitatively illustrated using the relationship, proposed by Stephens (1978), between two integral variables (cloud optical thickness and liquid water path) and the cloud effective radius, which is the main parameter to describe the microphysical properties of warm clouds.

$$\mathrm{COT} = \frac{3\mathrm{LWP}}{2\rho_{\mathrm{w}}\mathrm{CDR}} \tag{1}$$

where ρ_{w} is the density of water ($1\,\mathrm{g\,cm^{-3}}$) and CDR is defined as the ratio of the third to the second moment of the cloud droplet size distribution. Numerous analysis (e.g. Twomey, 1984; Kaufman and Fraser, 1997; Nakajima et al., 2001) have shown a relationship between the change in aerosol number concentration (N_a) within polluted clouds and the change in cloud droplet concentration (N_c) :

$$\delta \log N_{\mathrm{c}} = g\,\delta \log N_{\mathrm{a}} \tag{2}$$

where g is a sensitivity parameter.

ACPD
12, 14197–14246, 2012

From aircraft measurements over the ocean and land (Kaufman et al., 1991), g was found to be approximately equal to 0.7. Similarly, based on AVHRR measurements over the oceans, Nakajima et al., (2001) found a value of 0.5. In addition, the Aerosol Index (AI), defined as the product of the satellite-derived aerosol optical depth and Angstrom exponent (ANG), is a good proxy to quantify aerosol number concentration (Nakajima et al., 2001). It gives more weight to aerosol fine mode (between the most cloud active particles) than AOD alone. If cloud water amount can be assumed constant, Eqs. (1) and (2) yield

$$\delta \log \mathrm{CDR} = -\frac{\delta \log N_\mathrm{c}}{3} = -\frac{g}{3}\delta \log N_\mathrm{a} = -0.23\delta \log \mathrm{AI} \tag{3}$$

This means that a linear relationship is expected between the logarithm of the cloud droplet effective radius and the logarithm of the aerosol index, with a slope of −0.23, or −0.17 using the parametrization of Nakajima et al. (2001). In the following analysis, the strength of the different aerosol impact on cloud micro and macrophysics will be quantified by the slope value (called "sensitivity") of the log-log scale relationship between a given cloud property and aerosol index. According to Eq. (1), the strength of aerosol impact on cloud optical thickness is equal in magnitude, but opposite in sign, than that on cloud droplet size, as proposed by Twomey (1974, 1977).

On the other hand, if the assumption of constant liquid water path does not hold, the response of cloud optical thickness to aerosol increase can be expressed in logarithm form as

$$\frac{\delta \log \mathrm{COT}}{\delta \log \mathrm{AI}} = \frac{\delta \log \mathrm{LWP}}{\delta \log \mathrm{AI}} - \frac{\delta \log \mathrm{CDR}}{\delta \log \mathrm{AI}} \tag{4}$$

The strength of aerosol impact on cloud reflectance is then the combination of sensitivity of both the droplet size and cloud water content to the presence of aerosol.

ACPD
12, 14197–14246, 2012

Note that, with the objective of quantifying the aerosol impact on the Earth radiation budget, the COT is the proper proxy as it is well related to the cloud Albedo for a given sun zenith angle.

1.2.2 Relationship between cloud reflectance and particle size, in precipitating and non-precipitating clouds

Lohmann et al. (2000) used a general circulation model to explain differences in CDR-COT relationship between optically thin and thick clouds, as observed by Austin et al. (1999) off the coast of California, from AVHRR data. They show that precipitation works in the direction of keeping LWP constant with increasing cloud optical thickness (as a precipitating cloud grows, more water is removed through rain). According to equation (1), cloud droplet radius will show an inverse dependence on cloud optical thickness for a constant LWP.

$$\mathrm{CDR} \propto \mathrm{COT}^{-1} \tag{5}$$

On the other hand, in case of non-precipitating clouds, no specific assumption is made on LWP. From the general formula expressing cloud water amount as a function of cloud volume mean radius (approximated here by satellite retrieved droplet effective radius), droplet number concentration N and geometrical thickness H, we have

$$\mathrm{LWP} \approx \pi \rho_{\mathrm{w}} \frac{4}{3} \mathrm{CDR}^3 N H \tag{6}$$

Substituting Eq. (6) into Eq. (1), it follows that

$$\mathrm{COT} \approx 2 \pi \mathrm{CDR}^2 N H \tag{7}$$

In case of adiabatic clouds, the Liquid Water Content [$\mathrm{g\,m^{-3}}$] at altitude z above cloud base, LWC(z), increases almost linearly with altitude. LWP between cloud base

ACPD
12, 14197–14246, 2012

(cb) and cloud top (ct) can be easely calculated as

$$\mathrm{LWP} = \int_{Z_{\mathrm{cb}}}^{Z_{\mathrm{ct}}} \mathrm{LWC}(z)dz = \int_{Z_{\mathrm{cb}}}^{Z_{\mathrm{ct}}} c_{\mathrm{w}} z dz = \frac{1}{2} c_{\mathrm{w}} H^2 \quad (8)$$

Where c_w [kg m^{-4}] is the moist adiabatic condensation coefficient. It is almost constant in short stratocumulus clouds with geometrical thickness smaller than 1 km (Brenguier, 1991), depending slightly on the temperature (ranging between 1 and 2.5×10^{-3} g m^{-4} for T between 0° and 40 °C).

If a stratiform boundary layer cloud is not precipitating and not influenced by entrainment, there is ample observational evidence (Pawlowska and Brenguier, 2000) that cloud LWC vertical profile follows the so-called adiabatic cloud model. Putting together Eqs. (6), (7) and (8), the relationship between CDR and COT results

$$\mathrm{CDR} \propto \mathrm{COT}^{0.2}\, N^{0.5} \quad (9)$$

Adiabatic cloud droplet number concentration N is constant in a non-precipitating cloud, therefore droplet effective radius is expected to be an exponential function of cloud optical thickness, with exponent equal to 0.2. The comparison of (9) and (5) leads to the conclusion that change in sign of CDR-COT relationship slope from positive to negative can be attributed to the presence of non-precipitating versus precipitating clouds, respectively.

2 Dataset

Depending on the specific analysis, we use data acquired over whole South-East Atlantic region, within [4° N, 30° S; 14° W, 18° E], or limited to a smaller portion just off the coast of Angola, within [2° S, 15° S; 14° W, 18° E]. We used use data derived from the MODIS and CALIOP sensors, which are respectively onboard the AQUA and CALIPSO

ACPD
12, 14197–14246, 2012

satellites, both part of the so-called A-Train satellite constellation. They fly in close proximity on the same orbit at 705 km of altitude, within a lag of few minutes (Stephens et al., 2002) assuring near-coincident observations.

2.1 MODIS retrievals

MODIS aerosol retrieval algorithm over ocean (Tanré et al., 1997; Kaufman et al., 1997; Remer et al., 2009) uses seven spectral channels (0.66, 0.86, 0.47, 0.55, 1.24, 1.64, 2.12 µm). Level 2 (L2) products are organised into 5 min "granules". Only daytime data are considered for aerosol retrieval, and the products are generated at a resolution of $10\times10\,km^2$. Kaufman et al. (2005a) provide an in-depth analysis of error estimates over ocean and calculated that cloud contamination causes a maximum error in MODIS AOD equal to 0.02±0.005. Note that aerosol retrievals are only possible in case of clear or broken clouds condition, when MODIS can see between adjacent clouds.

MODIS retrievals of cloud effective radius and cloud optical depth L2 products (with a resolution of $1\times1\,km^2$), are derived using the six channels (King et al., 1998) at visible and near infrared wavelengths (0.66, 0.86, 1.24, 1.64, 2.12, 3.75). In this range of wavelengths, reflectance decreases when droplet size increases, for a constant cloud optical depth. Non-absorbing channel at 0.86 µm (over ocean) is chosen to minimize the surface contribution together with the base radiance at 2.12 µm (and eventually at 1.64 and 3.75 µm). Then, the couple of retrieved radiances are compared with a pre-computed Look Up Table (LUT). Bréon et al. (2005) show that a misunderstanding of 20 % in the cloud cover can lead to overestimate the cloud droplet radius by up to 2 µm, indicating that MODIS cloud retrieval algorithm is very sensitive to cloud heterogeneity. On the other hand, cloud retrievals based on the 0.86/2.1 µm combination are thought to be little affected by the presence of biomass burning and dust aerosols (Haywood et al., 2004). Cloud top properties, such as Cloud Top Pressure (CTP), are determined using radiances measured in spectral bands located within the broad 15 µm CO_2 absorption region (with a resolution of $5\times5\,km^2$). The accuracy of CTP estimates is found to be of 50 hPa of lidar determination in mono-layer clouds (Menzel et al., 2008; Garay

ACPD
12, 14197–14246, 2012

et al., 2008; Harshvardan et al., 2009). However, in case of atmospheric profiles with a strong inversion (e.g. marine stratocumulus areas), MODIS retrieval algorithms can place the cloud layer above the inversion, up to 200 hPa off its true position (1000–3000 m). Level 2 cloud fraction (at 5 km resolution) is derived from 1 km resolution cloud mask, equal to 0 in the absence of cloud and to 1 for cloudy conditions. It is calculated by computing the fraction of cloudy 1 km cloud mark pixels.

All atmospheric products are averaged on a 1×1 degree grid box (on daily, weekly, and monthly time scale), and are known as Level 3, L3, products. The QA "confidence" flag (whose value ranges from 3 to 0, where 3 means "good" quality and 0 means "bad" quality) is used for weighting L2 product onto a 1° grid low-resolution product.

In addition to aerosol and clouds, MODIS is able to retrieve fires and other thermal anomalies. MODIS Level 2 Active Fire Product (Giglio et al., 2010), MYD14, provides the position of active fires (latitude and longitude at center of fire pixel) with a high spatial resolution of 1 km.

2.2 CALIOP retrievals

CALIOP is the first spaceborne lidar optimized for aerosol and cloud measurements. It uses two orthogonally polarized channels at 532 nm and one at 1064 to measure the total backscattered signal (Winkler et al., 2007). Its footprint is very narrow, with a laser pulse diameter of 70 m on the ground (Khan et al., 2008), with a higher vertical resolution in the lower atmosphere than in and the upper layers, from 30 to 300 m (Winker et al., 2004). CALIPSO Level 1 products provide vertical profiles of Attenuated Backscatter values, while Level 2 products provide, among others, geophysical products at three different horizontal resolutions for clouds (333 m, 1 km and 5 km) and one for aerosol (5 km). Despite, non-perfect spatial coincidences, Kim et al. (2008) found a general agreement of CALIPSO estimates of cloud top and bottom heights with those derived from surface-based lidar observations, within 0.1 km.

ACPD
12, 14197–14246, 2012

2.3 MODIS-CALIPSO coincidences

Cloud parameters are obtained from MODIS Level 2 cloud product of collection C005 (MYD06_L2.C5) at 1 km resolution for *Cloud_Optical_Thickness*, *Cloud_Water_Path*, *Cloud_Effective_Radius* and 5 km resolution for *Cloud_Top_Pressure* and *Cloud_Fraction*. Aerosol *Effective_Optical_Depth_Best_Ocean* (0.55 µm) and *Angstrom_Exponent_1_Ocean* (0.55/0.86 µm), from MODIS Level 2 aerosol product of collection C005 (MYD04_L2.C5) at 10 km resolution, are used to estimate aerosol index. Cloud and aerosol layer altitudes are taken from CALIPSO Level 2 products. We make use of *Number_Layers_Found*, *Layer_Top_Altitude* and *Layer_Base_Altitude*, at 5 km resolution for both aerosol and clouds. MODIS and CALIPSO datasets are summarized in Table 1.

We use data acquired from June 2006 to December 2010. When CALIPSO detects the presence of mono-layer aerosol and cloud fields, we look for MODIS cloud and aerosol retrievals within a radius of 20 km from the CALIPSO target. Cases of clear-sky are not considered. Time-coincidence of retrievals is assured by the A-train coordinated orbits of Aqua and CALIPSO. This method is described schematically in Fig. 1.

Aerosol and cloud layers are assumed to be physically interacting when the vertical distance of aerosol bottom altitude from cloud top altitude is smaller than 100 m. Inversely, they are considered "well separated" if this distance is larger than 750 m. Aerosol and cloud layers with distance between 100 and 750 m are uncertain and excluded from our analysis, as are cases with the aerosol layer underneath the cloud layer.

In order to deal with shallow clouds only, cloud top pressure retrievals smaller than 600 hPa are excluded. In addition, COT smaller than 5 are also excluded because neither a clear distinction between aerosol and clouds, nor an accurate retrieval of cloud properties is reliably possible for optically thin clouds (Nakajima et al., 2001). Finally, cases of multilayer aerosol and clouds (retrievals can be ambiguous in such cases) and aerosol with top layer altitude larger than 10 km, are also excluded. All MODIS retrievals

ACPD
12, 14197–14246, 2012

within a 20 km radius from the CALIPSO target are averaged together, to provide single estimates of cloud and aerosol parameters for each CALIPSO shot. Cases with average COT larger than 35 and LWP larger than 300 g m^{-2} are excluded to avoid deep convective clouds.

3 Results

3.1 Aerosol production and transport over S-E Atlantic

MODIS Level 2 Active Fire Product for 2005 shows that fires over African continent mainly occur in the respective winter season of each hemisphere (Fig. 2). From November to March, fires are concentrated in the Sahel region, south the Sahara desert and north the Equator, extending approximately from the West coast of Mauritania to Ethiopia, crossing East-West almost the entire continent. From May to September fires are mainly located in Southern Africa, covering almost the entire subcontinent, between 0S and 20S. In April and October, fires are observed in both regions, north and south the Equator, but in much smaller numbers. Figure 2 show seasonal maps of wind speed and direction at 950 and 750 hPa (corresponding approximately at 0.6 and 2.5 km of altitude) for 2005, obtained from the monthly averaged data provided by the European Center for Medium-Range Weather Forecasts (ECMWF). Each arrow indicates the direction and intensity of the mean wind at that point. Wind speed is expressed in degrees per day so that arrow's length represents the distance travelled by the air in 24 h. Low level circulation at 950 hPa (green arrows), over South-East Atlantic between 0° S and 60° S, shows a N-NW circulation. During Apr-Jun and July–September, oceanic air masses from the South penetrate into the inner continent (over the Sahel region), while in Southern Africa the wind field is particularly weak. On the other hand, during Jan-Mar and Oct-Dec, the Gulf of Guinea becomes a convergence zone between the northward wind flow from South-East Atlantic and the southward flow from Sahel. At pressure levels of 850 (not shown in the figure) and 750 hPa (red ar-

ACPD
12, 14197–14246, 2012

rows), winds of Northern Hemisphere (between 20° N and 0° N) turn W-SW, while those of Southern Hemisphere (between 0° S and 20° S) turn W-NW. During April–June and July–September, the wind speed over Southern Africa increases consistently. Coincident with the peak of fire occurrence (biomass burning season), a strong easterly air transport from the inner continent over ocean is established. In the Northern Hemisphere, air masses from the Sahel are advected westward and southward over the Central Atlantic ocean and the Gulf of Guinea.

From this analysis, one may conclude that, during the winter fire season, the transport of biomass burning aerosol to the Gulf of Guinea is limited andmostly westward, only if the aerosol reaches a sufficient altitude. During the summer season, biomass burning aerosols from Southern Africa are transported efficiently towards the West, but not in the low atmospheric layers. Nevertheless, this analysis is based on seasonal mean circulation, and does not exclude other transports when the wind field does not follow the mean circulation. Another smoke transport mechanism has been observed by Haywood et al. (2008), analyzing data from the DABEX (Dust And Biomass-burning Experiment) field campaign. Over West Africa, mineral dust is transported southward from the Sahara desert (where a strong static stability prevent dust from mixing vertically and trap aerosol in a layer between 900 and 850 mbar), while biomass burning particles from savanna burning are subjected to a northward advection. When the two flows come in contact (over the convergence zone of low level winds, slightly north of 10° N) the hotter air mas from biomass burning overrides the cooler dust and is lifted to higher altitudes. With decreasing pressure level, local wind turns southward and westward, allowing for smoke transport over the Gulf of Guinea.

3.2 Aerosol distribution

We make use of MODIS Level 3 aerosol daily product over ocean (1° resolution) to analyze six years (2005–2010) of "seasonally" averaged maps of vertically integrated aerosol and cloud properties. Each year is divided in four time periods that differ from classical seasons, going from January to March, from April to June, from July

ACPD
12, 14197–14246, 2012

to September (biomass burning season of Southern Hemisphere) and from October to December.

Figures 3 and 4 show respectively aerosol index (AI) and Angstrom exponent (ANG) maps for 2005. While aerosol index is somewhat proportional to aerosol number concentration, ANG (computed from measurements at 550 and 865 nm) expresses the spectral dependence of aerosol optical depth and provide additional information on aerosol size (the larger the coefficient, the smaller the particle). An Angstrom exponent larger than 1 indicates that fine-mode particles (biomass burning aerosol) are the most abundant (Smirnov, 2002; Queface et al., 2003; Thieuleux, 2005). During January–March, AI reaches its maximum value over a small area in the northern part of the region, where it is smaller than AOD, as a result of an Angstrom exponent lower than one. Over the Gulf of Guinea, aerosol index ranges between 0.2 and 0.35, AOD between 0.5 and 0.8 and Angstrom exponent is around 0.5 or lower. Dust transported from the Sahara at relatively high altitude dominates the aerosol load. From April to June, when fires begin to occur in Southern Africa, aerosol load sensibly increases over coastal areas between the Gulf of Guinea and Angola. Aerosol index increases up to 0.5 and Angstrom exponent varies between 0.8 and 1.1, suggesting an easterly transport of smoke particles from Southern Africa over ocean, by trade winds. The heaviest aerosol concentration is observed during the biomass burning season (July–September), with AI values particularly elevated over a wide area off the coasts of Angola, between 0.5 and 1.5 (not visible in figure, showing value up to 0.7 only). Angstrom exponent over the whole area is generally larger than 0.7, exceeding unity (yellow and red points) near and off the coast of Angola. This most likely results from the abundant presence of biomass burning particles in the atmosphere. From October, fire occurrence in Southern Africa decreases significantly. Average values of AI and ANG during October–December are much lower than during July–August. Satellite data for 2006–2010 show a similar annual cycle of aerosol production and transport (with modest inter-annual variability compared to seasonal variations), dominated by two different regimes. The first one, from October to March, is characterized by opti-

ACPD
12, 14197–14246, 2012

cally thin aerosol layers (with AI generally below 0.2) and Angstrom exponents usually smaller than one, sign of a coarse-mode dominated regime. The second one, marked by the presence of larger concentrations of smaller particles, begins on April and culminates during the biomass burning season, when AI and ANG get both larger than one.

3.3 Aerosol impact on cloud droplet radius

In Fig. 5 coincident MODIS-CALIPSO estimates of cloud effective radius are averaged over constant bin of AI, from 0.02 to 0.5 (by step of 0.2), and reported in log-log scale. Cases of mixed or nearby aerosol and cloud layers are indicated in red, while case with aerosol above the cloud top are shown in blue. For a total of more than 15 000 valid retrievals, 56 % is representative of well separated layers, while 44 % of mixed ones. The study area is reduced to the smaller region off the coast of Angola, within [2° S, 15° S; 14° W, 18° E], where a previous analysis indicated that MODIS-CALIPSO coincidences are more homogeneously distributed than over the whole South-East Atlantic and mixed-unmixed analysis is less affected by local variation of meteorological parameters.

Mixed and unmixed case statistics converge to very similar CDR values when aerosol particle concentration is close to zero. With increasing AI, unmixed statistics does not show any significant correlation between changes in aerosol index and cloud droplet radius variations. CDR of clouds below the aerosol layer remains almost constant, close to 14–15 µm, at every aerosol regime. On the other hand, in case of cloud-aerosol mixing, CDR decreases by about 30 %, down to 11 µm, as AI varies from 0.02 to 0.5.

The strength of aerosol impact on CDR can be quantified by the linear regression slope of CDR-AI relationship in log-log scale. In good agreement with Twomey's hypothesis, Fig. 5 shows that the logarithmic relationship between CDR and AI in case of mixed and interacting layers is almost linear, with a correlation coefficient equal to −0.76. The strong CDR sensitivity to aerosol increase is expressed by the best-fit slope

ACPD
12, 14197–14246, 2012

of −0.15, five times smaller than in case of unmixed layers (−0.03), and in good agreement with the expected value (between −0.23 and −0.17).

3.4 Aerosol impact on cloud liquid water path

Averaging coincident MODIS-CALIPSO retrievals of liquid water path, within [2° S, 15° S], over constant bin of aerosol index, LWP-AI relationship (Fig. 6) is somewhat similar to CDR-AI. In case of mixed layers, LWP is decreased by 37 % (from 95 to 60 g m^{-2}) as AI increases from 0.03 to 0.5. The resulting linear slope in log-log scale is equal to −0.16. Otherwise, when the aerosol is located above cloud deck, LWP does not show any sensible dependence on aerosol concentration. Cloud water amount remains almost constant at approximately 80–90 g m^{-2} for all aerosol regimes and the resulting best linear fit slope is equal to −0.04.

In good agreement with expectation, mixed and unmixed layer relationships converge to a same LWP value (within statistical uncertainties), when AI decreases to very small values. We do not get the same result for the whole South-East Atlantic region [4° N, 30° S]. In the latter case, mixed statistics show that LWP would increase up to 110 g m^{-2}, for AI approaching to zero (while unmixed LWP would remains almost unaltered).

3.5 Aerosol impact on cloud optical thickness

In Fig. 7, coincident MODIS-CALIPSO estimates of cloud effective radius are averaged over constant bin of AI, from 0.02 to 0.5 (by step of 0.2), and reported in log-log scale. Both for mixed than unmixed layer cases, COT is little dependent on the aerosol index and shows variations that are not a clear function of the AI. A best fit among the rather scattered datapoints indicate that COT varies between 8.5 and 9.0. For AI values higher than 0.2, larger error bars indicate stronger statistical uncertainties than in case of lower aerosol loads, due to fewer measurements in the corresponding bin.

ACPD
12, 14197–14246, 2012

The low COT sensitivity to aerosol increase is significantly quantified by the log-log scale linear regression slope. When cloud and aerosol are mixed and interacting, the slope is particularly small, even slightly negative, equal to −0.02. A statistical uncertainties in the slope value equal to ±0.06, together with a linear correlation coefficient of $r = -0.47$, stress the large variability of COT and its little dependence on AI.

When aerosol and cloud layers are well separated, linear slope is very small and equal to 0.01 (with statistical error of ±0.04 and linear regression coefficient $r = 0.1$).

These results indicate that the impact of aerosol on the cloud optical thickness is hardly distinguishable from the noise.

3.6 Aerosol impact on cloud fraction

The cloud lifetime question is complex, and none of the hypothesis discussed in recent literature can uniquely explain the strong positive CLF-AI relationship, generally observed in satellite-derived relationships. As discussed above, the present analysis focuses on a specific area, that is unique by the presence of a layer of low clouds, often topped by large loads of biomass burning aerosols. We use MODIS Level 3 daily product (1 degree resolution) to compute linear regression of log-log scale CLF-AI relationship from 2005 to 2010. Resulting slopes are equal to 0.30–0.32, in good agreement with the satellite based results of Menon et al. (2008) and Quaas et al. (2009), but overestimating the values obtained from model simulation. For this mono-satellite analysis of cloud-aerosol relationship, where no distinction is made between mixed and unmixed statistics, we make use of MODIS retrievals acquired over the whole South-East Atlantic region.

Figure 8 shows cloud fraction estimates averaged over constant bin of cloud top pressure, from MODIS L3 daily product. We consider the whole 2005–2010 time period, sorting data from clean to polluted by AI and dividing them into six sample subsets, by step of 0.05. The mean AI value of each subset is reported in figure, indicated with the same color of the respective symbols. CLF correlates well with cloud top pressure, which is a proxy to roughly estimate cloud vertical development. Lower top pressure in-

ACPD
12, 14197–14246, 2012

dicates taller clouds that reach higher level of the atmosphere. Up to 700 hPa, the tallest clouds are characterized by the largest horizontal extension for all aerosol regimes. We can see a typical boomerang shape of CLF-CTP relationship, with a maximum at approximately 700 hPa. The diminution of cloud coverage for CTP larger than 700 hPa may indicate the occurrence of "high" clouds with larger cloud base altitude (in that case CTP is no more representative of cloud vertical extension) or multilayer cloud conditions (in that case the CTP-CLF relationship has to be considered meaningless). Note, however, that higher aerosol concentrations are characterized by larger cloud coverages at every pressure level.

On the other hand, CTP does not show any significant dependence on AI, if CLF is held constant. Figure 9 shows that CTP variations, averaged over constant bin of CLF, are very limited as AI varies between 0.03 and 0.37. For CLF larger than 60 %, they fall within the 2005–2010 annual variability. Slightly larger CTP variations, with increasing AI, are observed for CLF <60 %. In that case, larger error bars indicate fewer retrievals and averages with smaller representativity. For constant values of CLF, higher aerosol concentrations are not always associated to smaller top pressure, suggesting that CTP variations are not induced by aerosol-cloud interaction. In the hypothesis that aerosol does affect cloud structure, the results indicate that its primary effect is more likely to increase the horizontal extension than producing taller and more convective clouds.

In an attempt to isolate aerosol-induced from meteorological effects, we now analyze CLF-AI statistics from mixed (interacting) and well separated (not interacting) cloud-aerosol layers.

As shown from MODIS observations, larger CTP implies in average larger CLF, as well as larger CLF implies larger CTP, at least up to 700 hPa. We then believe it is better to compare CLF responses of clouds with similar vertical development. Cloud top pressure was found to be rather independent from aerosol interaction with cloud (Fig. 9). Keeping it constant, we exclude CLF variations caused by considering clouds with largely different CTP (due to different local meteorological conditions), without loosing any significant information on the strength of aerosol effect.

ACPD
12, 14197–14246, 2012

According to these considerations, mixed and unmixed MODIS-CALIPSO coincidences are sorted by CTP from low to high clouds, by step of 10 hPa, to provide a more accurate description of mixed and unmixed CLF sensitivity variation with cloud top pressure. CLF retrievals of each subset are averaged over constant bin of AI (from 0 to 0.7) by step of 0.2. The linear regression slope of each CLF-AI relationship in log-log scale is calculated and plotted in function of the correspondent CTP interval. This process is performed twice, once for the mixed (red) and once the unmixed case (blue), as shown in Fig. 10.

We make use of data from the whole South-East Atlantic [4° N, 30° S; 14° W, 18° E], including those regions excluded in previous mixed/not-mixed analysis. That is because the CTP sorting allows to minimize the effect of spatial heterogeneity of local meteorology on CLF-AI co-variation. Note that very high clouds are generally characterized by large cloud cover (almost equal to 100 % even at very low AI) that would obviously results in CLF-AI slopes equal to zero. Only cases with CLF lower than 97 % for AI = 0.01 are then considered.

Let define the sensitivity (S) to aerosol increase, of the cloud parameter k, as

$$S(k) = \frac{\delta \log k}{\delta \log \mathrm{AI}} \tag{10}$$

In case of mixed and interacting layers, cloud fraction sensitivity is small but positive, with no specific dependence on CTP. The error bars indicate the statistical uncertainties, as in Fig. 5. Apart from few points for CTP between 950 and 900 hPa, S(CLF) varies between 0.025 and 0.015 with an average value of 0.020.

In case of unmixed layers, CLF sensitivity variations with CTP are compelling. S(CLF) is almost zero when top layer altitude is larger than 2 km (CTP <800 hPa). As cloud top pressure exceeds 800 hPa, however, CLF dependence on AI becomes positive. S(CLF) undergoes a dramatic increase positively related to cloud top altitude diminution. In case of very low clouds (CTP = 970 Pa), CLF sensitivity reaches a maximum value of 0.10, five times larger than that observed in unmixed statistics for similar top pressure levels.

ACPD
12, 14197–14246, 2012

3.7 Aerosol impact on precipitation

To observe the effect of aerosol-cloud interaction on precipitation, we compare the CDR-COT relationship of mixed and unmixed cloud-aerosol layers. Cases of aerosol above cloud top are considered representative of clean cloud properties. In case of cloud-aerosol interaction, we only select data with AI larger than 0.09 to avoid very low aerosol regimes (when CDR values of interacting layers converge to those of unmixed ones) and consider mixed statistics as representative of polluted cloud properties. In addition, for AI >0.09, mixed and unmixed retrieval number concentrations result very similar over S-E Atlantic. This spatial homogeneity allows to consider all MODIS and CALIPSO coincidences retrieved over the whole region, whitin [4° N, 30° S; 14° W, 18° E]. Figure 11 shows cloud droplet effective radius estimates averaged over constant bin of cloud optical thickness, for clean (blue) and polluted clouds (red). In case of thin clouds (COT <10), the exponential fit for clean clouds returns an exponent equal to 0.80, which is four times larger than the expected value for adiabatic clouds (0.20) and larger than that obtained using MODIS daily retrievals (for the entire 2005–2010 dataset) over the same area (0.14; not shown). Similarly to the clean cloud case, thin polluted clouds show a positive CDR-COT relationship. The exponential fit returns an exponent equal to 0.59, little smaller than in case of well separated layers. This is consistent with Twomey's effect, according to which the effective radius of polluted droplets is smaller in average than that of unmixed and clean clouds. A cloud optical thickness of approximately 10 defines the threshold value beyond which CDR-COT relationship changes in sign, suggesting the occurrence of precipitation in both clean and polluted clouds. For COT between 9 and 11, CDR reaches a maximum value approximately between 17 µm (clean clouds) and 15.5 µm (polluted clouds), sufficiently large to allow for precipitation production. For COT ≥10 (optically thick clouds), the computed exponent of CDR-COT relationship in case of aerosol above clouds is negative and equal to −0.43, about half of value expected in case of constant LWP (−1). In case of polluted clouds, the calculated exponent is four times larger than for clean clouds and

ACPD
12, 14197–14246, 2012

equal to −0.11. This means that LWP enhancement with increasing COT is stronger in mixed than in well separated layer case. In the hypothesis that precipitation occurrence reduces the range of variation of liquid water path as cloud optical thickness increases, results indicate an inhibition of precipitation production as a consequence of aerosol-cloud interaction.

4 Discussion and interpretation

4.1 CDR-AI

The observed CDR decrease with increasing AI, only in case of mixed layers, is in good agreement with Twomey's theory and suggests a direct modification of cloud microphysics (decrease of the cloud droplet mean size) as a consequence of cloud interaction with aerosol particles, working as CCN. For strong aerosol loads, the mean difference in droplet radius between clean and polluted low clouds over South-East Atlantic is between 3 and 5 µm.

The spatial distribution of MODIS-CALIPSO coincidence number concentration (Fig. 12) shows that mixed and mixed case retrievals are mostly concentrated over a similar area. Satellite estimate are then expected to be representative of clouds developed under similar meteorological conditions. The observed differences in mixed and unmixed case statistics can be reliably interpreted as resulting from a real aerosol-induced effect, and not from changes in local meteorology. According to these consideration, the fact that CDR does not show any sensible evident change with AI increase, when aerosol is located above cloud top, suggests that meteorology has very little impact on statistics, while aerosol indirect effect is leading factor in governing the negative CDR-AI relationship, in case of interaction.

ACPD
12, 14197–14246, 2012

4.2 LWP-AI

Aerosol interaction with cloud field over South-East Atlantic produces a sensible decrease in cloud liquid water amount which is in clear contrast with the so-called "lifetime effect", proposed by Albrecht in 1989. He has been one of the first to theorize an increase in liquid water path amount with increasing aerosol concentration, as a consequence of precipitation suppression. The basic idea is that clouds in polluted air masses consist of more droplets that coalesce into raindrop less efficiently, leaving longer-lived clouds. In a more recent work, however, Ackerman et al. (2004), point out that aerosol-polluted boundary layers clouds are not generally observed to hold more water, but significantly less. They infer that cloud water response to precipitation suppression (due to increased droplet number concentration) is determined by the balance of two competitive factors: (1) moistening, from precipitation decrease, which tends to increase LWP with increasing aerosol concentration; (2) drying, from increasing entrainment of dry overlying air, which tends to decrease LWP. In their model simulation, they find that the entrainment rate [$cm\,s^{-1}$] always increases with increasing droplet number concentrations due to Twomey's effect. Only if overlying air is humid or droplet number concentration is very low, surface precipitation reduction is strong enough to dominate LWP response. In conclusion they identify relative humidity (RH) above boundary layer as the leading factor determining LWP response to changes in droplet concentration. If moisture is high enough, entrainment of air does not result in a dryness of cloud. Relative humidity is presently not detectable from satellites at high vertical resolution. However, the assumptions required by Ackerman's hypothesis are compatible with South-East Atlantic meteorology: during the biomass burning season of Southern Africa, large amount of aerosol particles are transported in elevated atmospheric layers by dry air masses, from inner Southern-Central Africa over ocean. It is reasonable to argue that aerosol-load air is dryer than that just above the inversion (there is no cloud, neither above the continent, nor above the ocean at the aerosol layer altitude). When aerosol mixes with underlying cloud field, increase in

ACPD
12, 14197–14246, 2012

cloud droplet number concentration (as a consequence Twomey's effect) may results in the observed LWP reduction, whose magnitude of $35\,g\,m^{-2}$ is comparable to that estimated by Ackerman et al. (2004) of $\sim 25\,g\,m^{-2}$, for RH of 10 %. If aerosol remains high in the atmosphere, well separated from cloud deck, no aerosol-cloud interaction is possible and LWP is expected to remain unaltered. This is in agreement with unmixed LWP trend of Fig. 6, very little dependent on aerosol concentration.

There are a number of implications of our findings. First of all the concept of *inhibition of precipitation*, commonly related to LWP increase according to the so often invoked Albrecht's hypothesis, can be misleading. The increase of number droplet concentrations and decrease of coalescence efficiency, in clouds polluted by sub-micrometers aerosol, may lead to large loss of LWP even if surface precipitation is reduced. Under such condition, COT-AI relationship can be positive or negative, depending on the competitive effect of simultaneous LWP and CDR variations with AI.

4.3 COT-AI

Previous results return a log-log scale CDR-AI linear slope, S(CDR), equal to −0.15 and a LWP-AI linear slope, S(LWP), of the same order and equal to −0.16. Equation (4) shows that the cloud optical thickness response to aerosol enhance can be estimated as the difference of these two parameters. Hence, in this particular case, no significant COT variations with aerosol enhancement are expected. Averaged values of COT over constant bin of AI, shown in Fig. 7 in log-log scale, are consistent with this estimate. The effect of liquid water path loss compensates the droplet size decrease. This finding has a strong radiative impact. Even if Twomey's hypothesis is valid at microphysics scale, aerosol-induced droplet size decrease does not produce any significant change in cloud reflectance, as a consequence of LWP loss. Consequently, also the resulting aerosol indirect radiative impact will be rather small.

ACPD
12, 14197–14246, 2012

4.4 CLF-AI

Unmixed relationships are supposed to reproduce CLF-AI co-variations induced by other causes than aerosol-cloud interaction, so where do these positive CLF-AI relationships come from? And why are they so strongly related with CTP?

When aerosol is located above clouds, an increase in low tropospheric stability (LTS) with increasing aerosol concentration would explain the positive CLF sensitivity observed in case of unmixed statistics. Low tropospheric stability is defined as the difference between the potential temperature of the free troposphere (700 hPa) and the surface, LTS = θ_{700}–θ_0 (Klein and Hartmann, 1993; Klein, 1997; Wood and Hartmann, 2006). The idea that cloud incidence tends to increase with increasing LTS goes back to the beginning of the twentieth century, with the stratocumulus studies of Blake (1928). In a more recent work, Klein and Hartmann (1993) find a linear relationship between seasonal mean LTS and low cloud amount, for regions in the subtropics.

Aerosol absorption of solar radiation may largely warm lower free troposphere if aerosol resides above cloud cover. Over the Atlantic ocean off the coast of Angola, Wilcox (2010) simulate the radiative effect of an aerosol layer (with single scattering albedo of 0.89±0.03) distributed between 1.5 and 4.2 km, with a peak at 3 km, and a stratocumulus cloud field (cloud optical thickness of 12) between 0.5 and 1.3 km (according to a statistics based on CALIPSO retrievals from July to September 2006–2008). For and AOD = 1, they find a peak of heating rate of 3.5±0.05 Kd^{-1} at pressure level slightly below 700 hPa, about 2.5 Kd^{-1} larger than in case of no aerosol. In addition, they find that the air temperature at 700 hPa in case of high smoke load is systematically warmer on average by nearly 1 K, than in case low smoke samples.

Unmixed statistics of Fig. 10 shows a positive CLF sensitivity to aerosol increase, smaller for higher cloud top altitudes but very large in case of shallow clouds. This suggests an aerosol-driven increased inversion strength, more effective at trapping moisture within the boundary layer, as leading factor in governing the (positive) relationship between low cloud coverage and concentration of absorbing aerosol above clouds.

ACPD
12, 14197–14246, 2012

However, when aerosol lies within the boundary layer, aerosol warming of air below the inversion is not expected to produce any increase in cloud cover. By means of large eddy simulation of stratocumulus clouds, Johnson et al. (2004) find that aerosol located within well-mixed boundary layer may in turn enhance entrainment of dry air and decrease cloud liquid water path and cloud fraction (semi-direct effect). In case of mixed cloud and aerosol layers, we observe a constant and positive CLF sensitivity (CLF increases with increasing aerosol concentration) in function of CTP (Fig. 10). This suggests that aerosol semi-direct effect is not dominant, it would at least induce a decrease but not an increase of cloud cover. Therefore, mixed statistics may reflect the effect of aerosol-cloud microphysical interaction in the way theorized by Albrecht, where precipitation suppression by cloud-active aerosols leads to longer-lived clouds.

In case of low clouds, unmixed CLF shows a strong dependence on aerosol concentration which is much larger than that observed for mixed cloud-aerosol layers. This result suggests that the so often invoked "swelling effect" is not probably the main factor governing the observed CLF and AI co-variations. Humidification of aerosol in the vicinity of clouds would induce to retrieve a stronger (at least equal) positive CLF sensitivity when aerosol particles are closer to clouds (mixed condition) and not farther (unmixed condition, with an aerosol-cloud distance threshold of 0.7 km).

This result is far from being an accurate estimate of the indirect aerosol effect on cloud cover. However, it indicates that if this effect exists, as mixed statistics suggest, its magnitude is just a small fraction of that 0.30–0.32 value obtained from MODIS daily product, probably dominated by other factors than a true aerosol-cloud microphysical interaction. Among them, the tendency of cloud fraction to correlate with aerosol-driven changes in low tropospheric stability seems to be the main actor.

4.5 CDR-COT

For both clean and polluted clouds, the change in sign of the CDR-COT relationship beyond COT = 10 indicates that precipitation mostly occurs in optically thick clouds, with average droplet radius between 17 and 15.5 µm. Examining cloud-precipitation in-

ACPD
12, 14197–14246, 2012

teraction by a combined use of radar and a solar/infrared radiometer on board of TRMM (Tropical Rainfall Measuring Mission), Kobayashi (2007) concludes that the largest effective radius for non-precipitating cloud is between 15–20 µm.

The calculated exponential fit for COT <10 returns exponential values (0.80 for clean and 0.59 for polluted clouds) sensibly smaller than expected for adiabatic clouds (0.20) and than observed using MODIS alone (0.14), from L3 daily product over the same area, for 2005–2010 (not shown). The difference between statistics resulting from MODIS-CALIPSO coincidences (retrieved at 5 km resolution) and MODIS observations (obtained merging 5 km onto 1 degree grid box) may indicate that warm clouds differ locally from adiabatic assumption, although the assumption is valid at larger scale.

If we look at LWP as a function of COT in case of optically thin clouds (not shown), cloud water amount increases rapidly with increasing optical thickness. As COT varies between 5 and 10, LWP increases from 40 to 120 $g\,m^{-2}$ (clean clouds) and from 40 to 90 $g\,m^{-2}$ (polluted). In conclusion, thin liquid clouds over the ocean have in average smaller water amount if they are mixed with polluted atmospheric layers (AI >0.09).

For COT = 10, the production of large droplets by coalescence-suppression processes is strongly inhibited in polluted environments, so that droplet radius of non-precipitating clouds is limited at ∼15.5 µm. For COT ≥10, the larger exponent of mixed case statistics suggest that polluted clouds rain less than clean ones. As cloud optical thickness increases from 10 to 19, the liquid water path of clean cloud is increased by 50 $g\,m^{-2}$ (from 120 to 170 $g\,m^{-2}$), while polluted liquid water path up to 90 $g\,m^{-2}$ (from 100 to 190 $g\,m^{-2}$). The percentage difference between clean and polluted LWP increases approximately from −15 to 15 %, as COT varies from 10 to 19. It is equal to zero for COT = 12.

Results seems to identify the presence of two different regimes. In case of thin clouds, aerosol enhanced entrainment of dry air at cloud top is the main mechanism in determining the LWP response to an increase in aerosol number concentration. This is a clear consequence of the specific meteorology of South-East Atlantic region, where extremely dry air is transported above cloud top, together with aerosol particles. Over

ACPD
12, 14197–14246, 2012

different regions, with different humid condition above the inversion, completely different results are expected. In case of thicker clouds, the LWP increase due to aerosol-induced suppression of collision-coalescence precesses dominates the water loss due to droplet evaporation at cloud top. If they are thick enough (COT >12), polluted clouds carry more water than clean ones.

5 Summary and conclusions

It is always difficult to assess the aerosol impact on cloud and precipitation from statistical analysis of satellite observations as the presence of aerosols correlates strongly with meteorological conditions. As a consequence, it is impossible to fully separate aerosol from meteorological contribution to the observed cloud property variations. In the present analysis we attempt to reduce this longstanding issue, making use of CALIPSO information to define whether or not aerosol and cloud layers observed by MODIS are mixed and presumably interacting. MODIS and CALIPSO fly in close proximity on the same sun-synchronous orbit and allow for coincident observations of the same Earth target.

We analysed the CDR-AI relationship, showing a decrease in droplet effective radius of mixed case clouds, approximately from 15-16 to 11 µm, as aerosol index varies from 0.02 to 0.5. When aerosol is located above cloud top, as it often occurs over South-East Atlantic, effective radius remains almost constant, close to 14–15 µm. Results are in good agreement with Twomey's hypothesis (Twomey, 1974; Twomey, 1977), according to which fine aerosol particles (efficient CCN) may largely increase cloud droplet number concentration. As a consequence, more numerous droplets lead to smaller mean droplet sizes, if cloud water amount remains constant. The fact that unmixed case statistics do not show any consistent correlation between changes in CDR and in AI, confirmed that aerosol-cloud interaction is the leading factor governing the observed cloud response.

ACPD
12, 14197–14246, 2012

Similar to CDR, we also performed statistics of LWP-AI and COT-AI, to investigate the response of cloud water amount and optical properties to changes in cloud microphysics. According to Twomey's theory, we expect an increase in cloud optical depth, when mean droplet size drops down (first indirect effect). This is only valid when assuming that the liquid water path is constant.

Contradictory with this hypothesis, coincident MODIS-CALIPSO observations show a clear decrease in LWP, from 90–100 to 60 g m^{-2}, as AI varies between 0.02 to 0.5, in case of interaction of cloud and aerosol layers. LWP remains almost constant with increasing AI, when aerosol is above cloud top and cannot interact with underlying layer. We infer that aerosol-induced LWP diminution is due to the enhancement of dry air entrainment, that enhances droplet evaporation at cloud top. Dry air is presumably transported by trade winds from inner continent over the ocean, together with aerosol particles. In Southern African, absolute humidity can reach extremely low values during the biomass burning season.

Cloud optical thickness response to aerosol enhancement, resulting from the balance of LWP depletion and CDR increase, is very weak in both cases of mixed and unmixed layers.

Although aerosol impact on cloud microphysics is strong, the effect on cloud optical properties is not significant, as liquid water path assumption is not valid over the study area. Twomey's effect on cloud reflectance cannot be demonstrated over this particular area. Rather it appears that the very clear impact of aerosol on the cloud microphysics is somewhat compensated by the impact on the cloud liquid water path. To address this issue further, independent measurements of LWP such as those from other instruments of the A-Train (AMSR-E and CLoudsat) would be most useful. Indeed, MODIS algorithm calculates LWP directly from CDR and COT estimates and is therefore not independent.

The cloud fraction response to aerosol-induced changes in LWP has been investigated from the analysis of CLF-AI relationship. We found that CLF is strongly correlated to cloud top pressure, which is a good proxy to approximately estimate cloud vertical

ACPD
12, 14197–14246, 2012

extension. If clouds form under the same quantity of aerosol but different meteorological condition, they would develop differently and present different vertical extensions. Since changes in local meteorology can produce spurious correlation between changes in CLF and AI, we decided to minimize the effect of considering clouds under different meteorological conditions sorting data by CTP. In that way, differences between mixed and unmixed case statistics can be reliably attributed to the effect of aerosol-cloud interaction.

In case of mixed layers, we found a positive CLF sensitivity equal to 0.02, for cloud top altitude at every pressure level. This value is much smaller that those generally found from satellite-based observations (Menon et al., 2008; Quaas et al., 2009). Indeed, when aerosol lies above cloud top, cloud fraction sensitivity is large for lower clouds, (up to 0.09 at CTP = 970 hPa), decreasing with decreasing CTP (almost zero at CTP = 750 hPa). Absorbing particle above cloud top may largely warm the atmosphere and increase the low tropospheric stability. The enhancement of LTS increases the strength of inversion, suppressing cloud vertical extent and maintaining a well-mixed and moist boundary layer, providing favorable condition to low cloud cover enhancement over ocean. Aerosol radiative effect is then supposed to be a major driver of cloud fraction increase, in case of unmixed layers.

Aerosol impact on precipitation and cloud life-cycle has been analyzed as well. Previous studies (Lohmann et al., 2000) have shown that occurrence of precipitation is detectable by studying the relationship between CDR and COT. A change in the sign of the curve slope can reliably be attributed to the transition from non-precipitating to precipitating clouds. For non-precipitating clouds, CDR is expected to be a positive exponential function of COT. For COT <10, the calculated exponent of CDR-COT relationship is equal to 0.59 in case of mixed layers, and equal to 0.80 in case on unmixed, whereas the theoretical value for adiabatic clouds is 0.20. We then observe that optically thin clouds over South-East Atlantic are generally non-precipitating, but showing a certain deviation from the adiabatic assumption, at least at local scale (5 km resolution). On the other hand, precipitating clouds are expected to show an exponential

ACPD
12, 14197–14246, 2012

relationship of CDR as a function of COT, with negative exponent. According to theory, the more precipitating the cloud the smaller is the exponent. In case of mixed layers, the calculated exponent is −0.11, while in case of aerosol above clouds the exponent is four times smaller and equal to −0.43 (−0.47, using MODIS L3 daily product alone). We infer an aerosol-induced effect on precipitation, which is inhibited in polluted clouds. This is expected to be a consequence of collision-coalescence suppression, by aerosol-driven change in cloud microphysics. Smaller droplets convert to rain less efficiently.

In conclusion, optically thin clouds carry more water in clean than in polluted environments. As COT goes over 10, clouds begin to precipitate and clean ones precipitate more. As a consequence, more water is removed through rain. Beyond a COT value of approximately 12, polluted clouds are generally characterized by higher LWP than clean ones. Results are in good agreement with Albrecht's hypothesis (Albrecht, 1989) and LWP response to AI enhancement seems governed by two opposite effects. The first one is a drying effect due to aerosol-induced enhanced entrainment of dry air at clouds top, that leads to droplet evaporation and is dominant in optically thin clouds. The second one is a moistening effect, due to aerosol decrease of collision-coalescence processes, that leads to precipitation suppression and increased cloud water amount, dominant in optically thicker clouds.

Present results evidence that aerosol intrusion into low cloud systems can suppress precipitation and lead to longer-lived clouds, stressing a further possible pathway by which human activity is associated to changes in hydrologic cycle and more generally to climate change. Further work is needed to better quantify pollution impact on rain development and, more generally, on low cloud coverage enhancement (with and without physical interaction between aerosol and cloud droplets). In order to address this issue, the use of precipitable water retrievals together with low tropospheric stability estimates and independent measurements of the cloud liquid water content would be a valuable addition to MODIS-CALIPSO statistics.

ACPD
12, 14197–14246, 2012

Acknowledgements. We are grateful to the ICARE centre for providing computing resources and easy access to data, acquired by NASA and CNES satellites.

References

Ackerman, A. S., Kirkpatrick, M. P., Stevens, D. E., and Toown, O. B.: The impact of humidity above stratiform clouds on indirect aerosol climate forcing. Nature, 432, 1014–1017, doi:10.1038/nature03174, 2004.

Albrecht, B. A.: Aerosols, Cloud Microphysics, and Fractional Cloudiness. Science, 245, 1227–1230, 1989.

Andreae, M. O. and Merlet, P.:. Emission of trace gases and aerosols from biomass burning, Global Biogeochem. Cy., 15, 955–966, 2001.

Austin, P. H., Szczodrak, M., and Lewis, G. M.: Spatial variability of satellite-retrieved optical depth and effective radius in marine stratocumulus clouds, in Proceedings of the 10th Conference on Atmospheric Radiation, Madison, Wisconsin, Amer. Meteorol. Soc., 237–240, 1999.

Brenguier, J. L.: Parameterization of the condensation process: A theoretical approach. J. Atmos. Sci., 48, 264–282, 1991.

Bréon, F. M. and Doutriaux-Boucher, M.: A comparison of cloud droplet radii measured from space, IEEE Trans Geosci. Remote Sens., 43, 1796–1805, 2005.

Bréon, F.-M., Tanré, D., and Generoso, S.: Effect of aerosols on cloud droplet size monitored from satellite, Science, 295, 834–838, doi:10.1126/science.1066434, 2002.

Costantino, L. and Bréon, F.-M.: Analysis of aerosol-cloud interaction from multi-sensor satellite observations, Geophys. Res. Lett., 37, L11801, doi:10.1029/2009GL041828, 2010.

Edwards, D. P., Emmons, L. K., Gille, J. C., Chu, A., Attie, J. L., Giglio, L., Wood, S. W., Haywood, J., Deeter, M. N., Massie, S. T., Ziskin, D. C., and Drummond, J. R.: Satellite-observed pollution from Southern Hemisphere biomass burning, J. Geophys. Res.-Atmos., 111, D14312, doi:10.1029/2005jd006655, 2006.

Feingold, G., Eberhard, W. L., Veron, D. E., and Previdi, M.: First measurements of the Twomey indirect effect using ground-based remote sensors, Geophys. Res. Lett., 30, 1287, doi:10.1029/2002GL016633, 2003.

ACPD

12, 14197–14246, 2012

Garay, M. J., de Szoeke, S. P., and Moroney, C. M.: Comparison of marine stratocumulus cloud top heights in the southeastern Pacific retrieved from satellites with coincident ship-based observations, J. Geophys. Res., 113, D18204, doi:10.1029/2008JD009975, 2008.

Giglio, L., Descloitres, J., Justice, C. O., and Kaufman, Y.: An enhanced contextual fire detection algorithm for MODIS, Remote Sens. Environ., 87, 273–282. doi:10.1016/S0034-4257(03)00184-6, 2003.

Han, Q., Rossow, W. B., Zeng, J., and Welch, R.: Three different behaviors of liquid water path of water clouds in aerosol-cloud interactions, 59, 726–735, doi:10.1175/1520-0469(2002)059, 2002.

Harshvardhan, Z. G., Di Girolamo, L., and Green, R. N.: Satellite-observed location of stratocumulus cloudtop heights in the presence of strong inversions. IEEE Trans. Geosci. Remote Sens., 47, doi:10.1109/TGRS.2008, 2005406, 1421–1428, 2009.

Haywood, J. M., Pelon, J., Formenti, P., Bharmal, N., Brooks, M., Capes, G., Chazette, P., Chou, C., Christopher, S., Coe, H., Cuesta, J., Derimian, Y., Desboeufs, K., Greed, G., Harrison, M., Heese, B., Highwood, E. J., Johnson, B., Mallet, M., Marticorena, B., Marsham, J., Milton, S., Myhre, G., Osborne, S. R., Parker, D. J., Rajot, J.-L., Schulz, M., Slingo, A., Tanré, D., and Tulet, P.: Overview of the Dust and Biomass-burning Experiment and African Monsoon Multidisciplinary Analysis Special Observing Period-0, J. Geophys. Res., 113, D00C17, doi:10.1029/2008JD010077, 2008.

Haywood, J. M., Osborne, S. R., and Abel, S. J.: The effect of overlying absorbing aerosol layers on remote sensing retrievals of cloud effective radius and cloud optical depth, Q. J. Roy. Meteorol. Soc., 130, 779–800, 2004.

Ichoku, C., Remer, L. A., Kaufman, Y. J., Levy, R., Chu, D. A., Tanré, D., and Holben, B. N.: MODIS observation of aerosols and estimation of aerosol radiative forcing over southern Africa during SAFARI 2000, J. Geophys. Res., 108, 8499, doi:10.1029/2002JD002366, 2003.

Kaufman, Y. J. and Fraser, R. S.: The effect of smoke particles on clouds and climate forcing, Science, 277, 1636–1639, 1997.

Kaufman, Y. J., Fraser, R. S., and Mahoney, R. L.: Fossil fuel and biomass burning effect on climate-Heating or cooling?, J. Clim., 4, 578–588, 1991.

Kaufman, Y. J., Tanré, D., Remer, L. A., Vermote, E. F., Chu, A., and Holben, B. N.: Operational remote sensing of tropospheric aerosol over land from eos moderate resolution imaging spectroradiometer, J. Geophys. Res.-Atmos., 102, 17051–17067, 1997.

ACPD
12, 14197–14246, 2012

Kaufman, Y. J., Remer, L., Tanré, D., Li, R., Kleidman, R., Mattoo, S., Levy, R., Eck, T., Holben, B., Ichoku, C., Martins, J., and Koren, I.: A critical examination of the residual cloud contamination and diurnal sampling effects on MODIS estimates of aerosol over ocean, IEEE Trans. Geosci. Remote Sens., 43, 2886–2897, 2005a.

Kaufman, Y. J., Koren, I., Remer, L. A., Rosenfeld, D., and Rudich, Y.: The effect of smoke, dust and pollution aerosol on shallow cloud development over the Atlantic Ocean, Proc. Natl. Acad. Sci. USA, 102, 11207–11212, doi:10.1073/pnas.0505191102, 2005b.

Kahn, R. A., Chen, Y., Nelson, D. L., Leung, F.-Y., Li, Q., Diner, D. J., and Logan, J. A.: Wildfire smoke injection heights; two perspectives from space, Geophys. Res. Lett, 35, L04809, doi:10.1029/2007GL032165, 2008.

Kim, S.-W., Berthier, S., Raut, J.-C., Chazette, P., Dulac, F., and Yoon, S.-C.: Validation of aerosol and cloud layer structures from the space-borne lidar CALIOP using a ground-based lidar in Seoul, Korea, Atmos. Chem. Phys., 8, 3705–3720, doi:10.5194/acp-8-3705-2008, 2008.

King, M. D., Tsay, S. C., Platnick, S. E., Wang, M., and Liou, K. N.: Cloud retrieval algorithms for MODIS: Optical thickness, effective particle radius, and thermodynamic phase, MODIS Algorithm Theoretical Basis Document, ATBD-MOD-05, 78 pp., 1997.

Labonne, M., Bréon, F.-M., and Chevallier, F.: Injection height of biomass burning aerosols as seen from a spaceborne lidar, Geophys. Res. Lett., 34, L11806, doi:10.1029/2007GL029311, 2007.

Lebsock, M. D., Stephens, G. L., and Kummerow, C.: Multisensor satellite observations of aerosol effects on warm clouds, J. Geophys. Res., 113, D15205, doi:10.1029/2008JD009876, 2008.

Lee, S. S., Penner, J. E., and Saleeby, S. M.: Aerosol effects on liquid-water path of thin stratocumulus clouds, J. Geophys. Res., 114, D07204, doi:10.1029/2008JD010513, 2009.

Loeb, N. G. and Schuster, G. L.: An observational study of the relationship between cloud, aerosol and meteorology in broken low-level cloud conditions, J. Geophys. Res., 113, D14214, doi:10.1029/2007JD009763, 2008.

Lohmann, U., Tselioudis, G., and Tyler, C.: Why is the cloud albedo-particle size relationship different in optically thick and optically thin clouds?, Geophys. Res. Lett., 1099, 1102, doi:10.1029/1999GL011098, 2000.

ACPD
12, 14197–14246, 2012

Marshak, A., Wen, G., Coakley, J., Remer, L., Loeb, N. G., and Cahalan, R. F.: A simple model for the cloud adjacency effect and the apparent bluing of aerosols near clouds J. Geophys. Res., 113, D14S17, doi:10.1029/2007JD009196, 2008.

Matsui T., and Pielke Sr., R.: Measurement-based estimation of the spatial gradient of aerosol radiative forcing. Geophys. Res. Lett., 33, L11813, doi:10.1029/2006GL025974, 2006.

Menon, S., Del Genio, A. D., Kaufman, Y., Bennartz, R., Koch, D., Loeb, N., and Orlikowski, D.: Analyzing signatures of aerosol-cloud interactions from satellite retrievals and the GISS GCM to constrain the aerosol indirect effect, J. Geophys. Res., 113, D14S22, doi:10.1029/2007JD009442, 2008.

Menzel, W. P., Frey, R. A., Zhang, H., Wylie, D. P., Moeller, C. C., Holz, R. E., Maddux, B., Baum, B. A., Strabala, K. I., Gumley, L. E.: MODIS global cloud-top pressure and amount estimation: Algorithm description and results, J. Appl. Meteorol. Climatol., 47, 1175–1198, 2008.

Nakajima, T., Higurashi, A., Kawamoto, K., and Penner, J. E.: A possible of correlation between satellite-derived cloud and aerosol microphysical parameters, Geophys. Res. Lett., 28, 1171–1174, 2001.

Pawlowska, H. and Brenguier, J. L.: Microphysical properties of stratocu mulus clouds during ACE-2, Tellus, Ser. B, 52, 867–886, 2000.

Quaas, J., Ming, Y., Menon, S., Takemura, T., Wang, M., Penner, J. E., Gettelman, A., Lohmann, U., Bellouin, N., Boucher, O., Sayer, A. M., Thomas, G. E., McComiskey, A., Feingold, G., Hoose, C., Kristjánsson, J. E., Liu, X., Balkanski, Y., Donner, L. J., Ginoux, P. A., Stier, P., Grandey, B., Feichter, J., Sednev, I., Bauer, S. E., Koch, D., Grainger, R. G., Kirkevåg, A., Iversen, T., Seland, Ø., Easter, R., Ghan, S. J., Rasch, P. J., Morrison, H., Lamarque, J.-F., Iacono, M. J., Kinne, S., and Schulz, M.: Aerosol indirect effects – general circulation model intercomparison and evaluation with satellite data, Atmos. Chem. Phys., 9, 8697–8717, doi:10.5194/acp-9-8697-2009, 2009.

Quaas, J., Stevens, B., Stier, P., and Lohmann, U.: Interpreting the cloud cover – aerosol optical depth relationship found in satellite data using the general circulation model, Atmos. Chem. Phys., 6129–6135. doi:10.5194/acp-10-6129-2010, 2010.

Quaas, J., Boucher, O., Bellouin, N., and Kinne, S.: Satellite-based estimate of the direct and indirect aerosol climate forcing, J. Geophys. Res., 113, D05204, doi:10.1029/2007JD008962, 2008.

ACPD
12, 14197–14246, 2012

Queface, A. J., Piketh, S. J., Annegarn, H. J., Holben, B. N., and Uthui, R. J.: Retrieval of aerosol optical thickness and size distribution from the CIMEL sun photometer over Inhaca island, Mozambique, J. Geophys. Res., 108, 8509, doi:10.1029/2002JD002374, 2003.

Remer, L. A., Tanré, D., Kaufman, Y., Levy, R., and Mattoo, S.: Algorithm for Remote Sensing of Tropospheric Aerosol from MODIS: Collection 005, Rev 2, 97 pp, available at: http://modis-atmos.gsfc.nasa.gov, last access: 14 November 2009, February 2009.

Sekiguchi, M., Nakajima, T., Suzuki, K., Kawamoto, K., Higurashi, A., Rosenfeld, D., Sano, I., and Mukai, S.: A study of the direct and indirect effects of aerosols using global satellite data sets of aerosol and cloud parameters, J. Geophys. Res., 108, 4699, doi:10.1029/2002JD003359, 2003.

Smirnov, A., Holben, B. N., Kaufman, Y. J., Dubovik, O., Eck, T. F., Slutsker, I., Pietras, C., Halthore, R. N.: Optical properties of atmospheric aerosol in maritime environments, J. Atmos. Sci., 59, 501–523, 2002.

Stephens, G., Vane, D. G., Boain, R. J., Mace, G. G., Sassen, K., Wang, Z., Illingworth, A. J., O'Connor, E. J., Rossow, W. B., Durden, S. L., Miller, S. D., Austin, R. T., Benedetti, A., and Mitrescu, C. and The CloudSat Science Team: The CloudSat mission and the A-Train, B. Am Meteorol. Soc., 83, 1771–1790, 2002.

Stephens, G. L.: Radiation Profiles in Extended Water Clouds – II: Parameterization Schemes, J. Atmos. Sci., 12, 2123–2132, 1978.

Stevens, B. and Feingold, G.: Untangling aerosol effects on clouds and precipitation in a buffered system, Nature, 461, 607–613, doi:10.1038/nature08281, 2009.

Tanré, D., Kaufman, Y. J., Herman, M., and Mattoo, S.: Remote sensing of aerosol properties over oceans using the MODIS/EOS spectral radiances, J. Geophys. Res.-Atmos., 102, 16971–16988, 1997.

Thieuleux, F., Moulin, C., Bréon, F. M., Maignan, F., Poitou, J., and Tanré, D.: Remote sensing of aerosols over the oceans using MSG/SEVIRI imagery, Ann. Geophys., 23, 3561–3568, doi:10.5194/angeo-23-3561-2005, 2005.

Twohy, C. H., Petters, M. D., Snider, J. R., Stevens, B., Tahnk, W., Wetzel, M., Russell, L., and Burnet, F.: Evaluation of the aerosol indirect effect in marine stratocumulus clouds: Droplet number, size, liquid water path, and radiative impact, J. Geophys. Res., 110, D08203, doi:10.1029/2004JD005116, 2005.

Twomey, S.: Pollution and the planetary albedo, Atmos. Environ., 8, 1251–1256, 1974.

ACPD
12, 14197–14246, 2012

Twomey, S.: The influence of pollution on the shortwave albedo of clouds, J. Atmos. Sci., 34, 1149–1152, 1977.
Twomey, S.: An assessment of the impact of pollution on global cloud albedo, Tellus, Ser. B, 36, 356–366, 1984.
Varnai, T. and Marshak, A.: MODIS observations of enhanced clear sky reflectance near clouds, Geophys. Res. Lett. 36, L06807, doi:10.1029/2008GL037089, 2009.
Warner, J.: A reduction in rainfall associated with smoke from sugar-cane fires: an inadvertent weather modification, J. Appl. Meteorol., 7, 247–251, 1968.
Warner, J. and Twomey, S. A.: The production of cloud nuclei by cane fires and the effect on cloud droplet concentration, J. Atmos. Sci., 24, 704–706, 1967.
Wen, G., Marshak, A., and Cahalan, R. F.: Importance of molecular Rayleigh scattering in the enhancement of clear sky reflectance in the vicinity of boundary layer cumulus clouds, J. Geophys. Res., 113, D24207, doi:10.1029/2008JD010592, 2008.
Winker, D. M., Hunt, B. H., and McGill, M. J.: Initial performance assessment of CALIOP, Geophys. Res. Lett., 34, L19803, doi:10.1029/2007GL030135, 2007.
Winker, D. M., Hunt, W. H., and Hostetler, C. A.: Status and performance of the CALIOP lidar, Proc. SPIE Int. Soc. Opt. Eng., 5575, 8–15, 2004.

ACPD
12, 14197–14246, 2012

Table 1. Level 2 product used to characterize cloud and aerosol properties from MODIS-CALIPSO coincident retrievals.

Product	Dataset	Horizontal Resolution	Sensor (Satellite)
Aerosol (05kmALay) and cloud (05kmCLay)	*Number_Layers_Found*	5 km	CALIOP (CALIPSO)
	Layer_Top_Altitude	5 km	
	Layer_Base_Altitude	5 km	
Aerosol (MYD04_L2.C5)	*Effective_Optical_Depth_Best_Ocean* (0.55 µm)	10 km	MODIS (Aqua)
	Angstrom_Exponent_1_Ocean (0.55/0.86 µm)	10 km	
Cloud (MYD06_L2.C5)	*Cloud_Optical_Thickness*	1 km	
	Cloud_Water_Path	1 km	
	Cloud_Effective_Radius	1 km	
	Cloud_Top_Pressure	5 km	
	Cloud_Fraction	5 km	

ACPD
12, 14197–14246, 2012

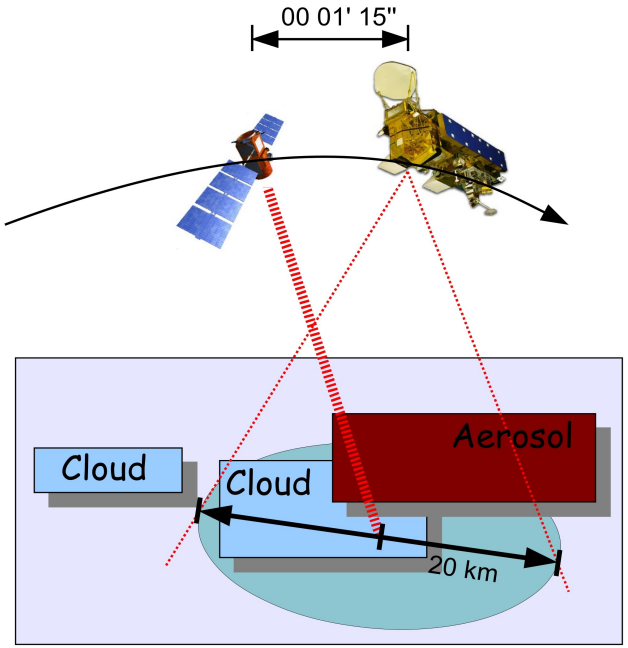

Fig. 1. Scheme of CALIPSO-MODIS coincidence methodology. When CALIPSO detects the presence of single-layer aerosol and cloud fields, we look for MODIS retrievals within a radius of 20 km from CALIPSO target, within a lag of very few minutes.

ACPD
12, 14197–14246, 2012

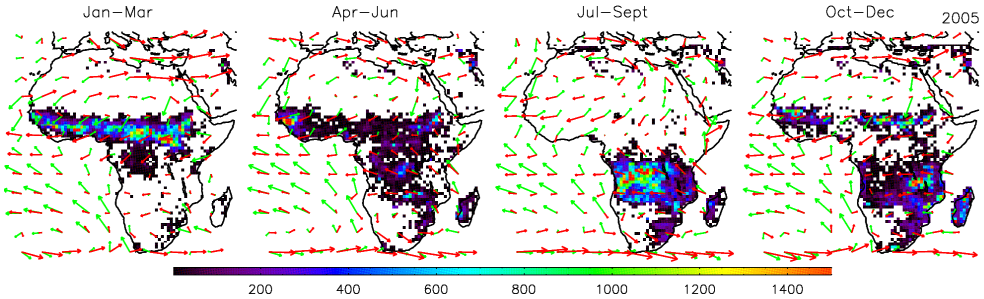

Fig. 2. Maps of fire occurrence for 2005, according to MODIS Active Fire Product. Color-scale represents the number of active fires detected during each time period, at a nominal resolution (at nadir) of 1 km, within a 1°×1° gird box. Wind fields at 950 (green) and 750 (red) hPa (corresponding approximately to 600 m and 2.5 km of altitude) for 2005 are overplotted on the figure. Seasonal wind maps are obtained from monthly averaged data provided by the European Center for Medium-Range Weather Forecasts (ECMWF). Arrows indicate the direction and intensity of the mean wind at that point. Wind speed is expressed in degrees per day so that arrow's length shows the distance travelled by the air in 24 h.

ACPD
12, 14197–14246, 2012

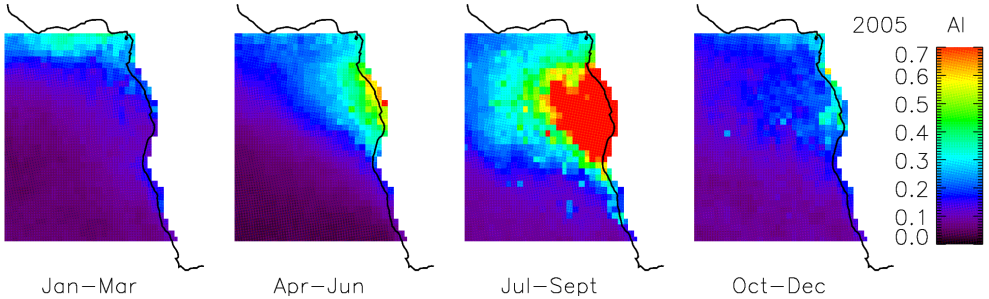

Fig. 3. Maps of seasonally averaged measurements of Aerosol Index (AI), for 2005. AI seasonal variability is high but somewhat different from that of AOD, because aerosol composition and hence Angstrom exponent vary during the year.

ACPD
12, 14197–14246, 2012

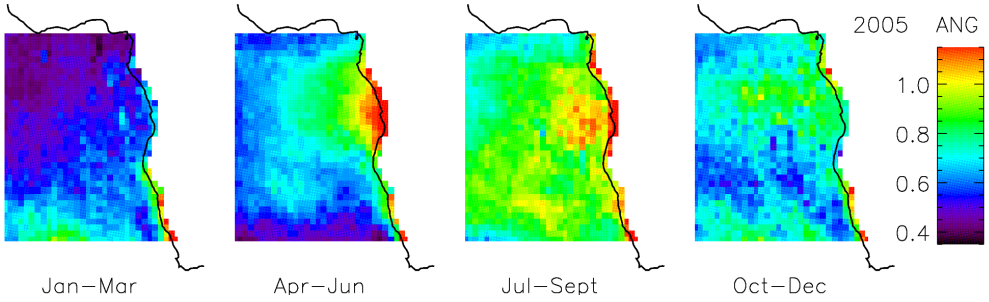

Fig. 4. Maps of seasonally averaged measurements of Angstrom exponent (ANG), for 2005.

ACPD
12, 14197–14246, 2012

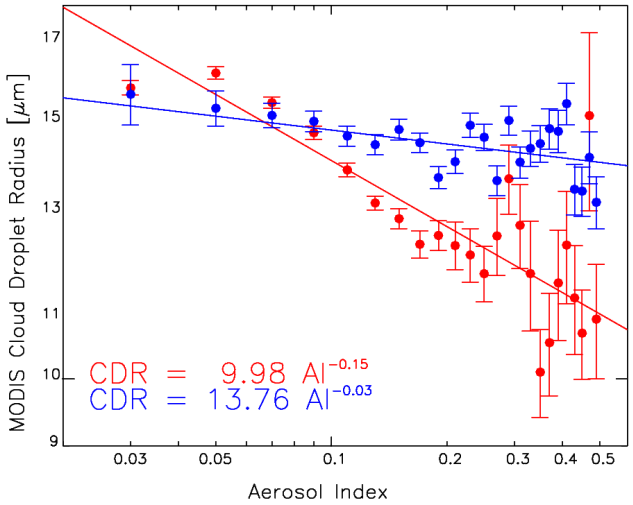

Fig. 5. Cloud Droplet Radius (CDR) retrievals averaged over constant bin of Aerosol Index (AI) in log-log scale, for cases of well separated cloud and aerosol layers (blue) and mixed and interacting layers (red), in the region within [2° S, 15° S; 14° W, 18° E]. Error bars represent the confidence level of the mean values if one assumes independent data. They are calculated as $\sigma/(n-2)^{1/2}$, where n is the number of CDR measurements within the bin and σ their standard deviation.

ACPD
12, 14197–14246, 2012

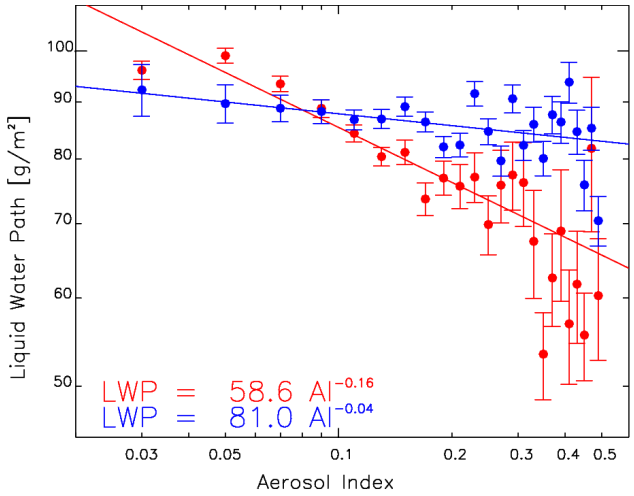

Fig. 6. Liquid Water Path (LWP) retrievals averaged over constant bin of Aerosol Index (AI) in log-log scale, for cases of well separated (blue) and interacting (red) cloud-aerosol layers, in the region within [2° S, 15° S; 14° W, 18° E]. The error bars indicate the statistical uncertainties as in Fig. 5.

ACPD
12, 14197–14246, 2012

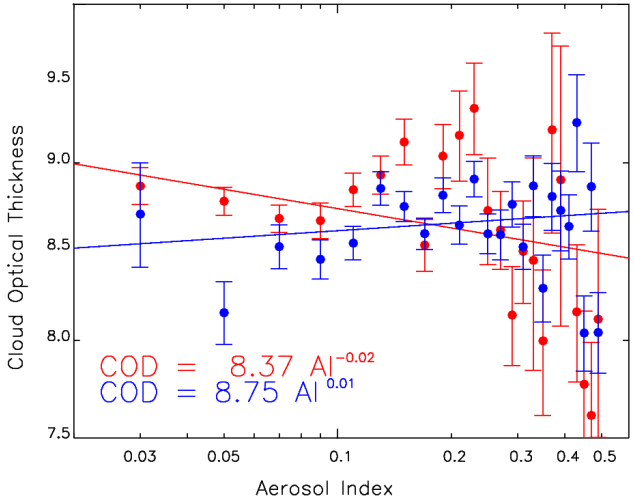

Fig. 7. Cloud Optical Thickness (COT) retrievals averaged over constant bin of Aerosol Index (AI) in log-log scale, for cases of well separated (blue) and mixed (red) cloud-aerosol layers, in the region within [2° S, 15° S; 14° W, 18° E]. The error bars indicate the statistical uncertainties as in Fig. 5.

ACPD
12, 14197–14246, 2012

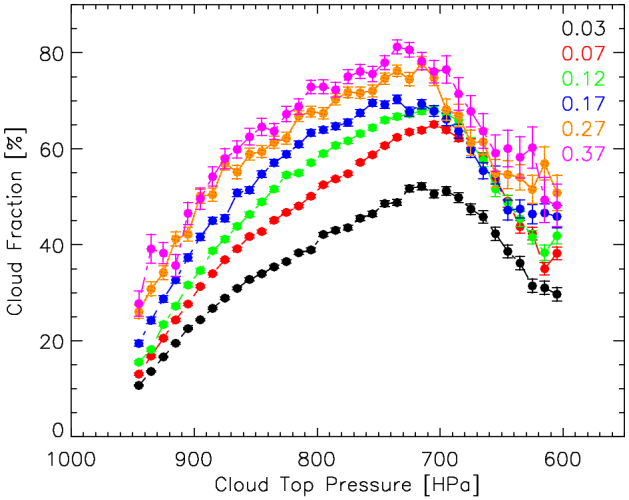

Fig. 8. CLF-CTP relationships from MODIS daily products, at 1 degree resolution, in the region within [4° N, 30° S; 14° W, 18° E]. The whole 2005–2010 dataset is sorted by AI, from little to high polluted atmosphere, by step of 0.1. Colors represent different aerosol index intervals (mean AI values are reported in figure). The error bars indicate the statistical uncertainties as in Fig. 5.

ACPD
12, 14197–14246, 2012

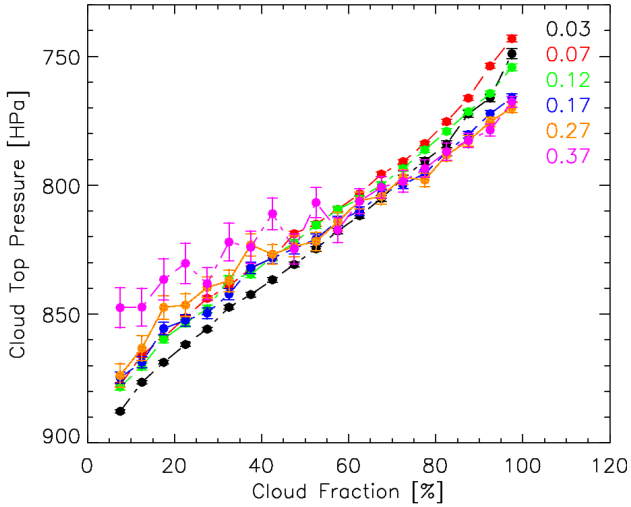

Fig. 9. CTP-CLF relationships from MODIS daily products, at 1 degree resolution, in the region within [4° N, 30° S; 14° W, 18° E]. The whole 2005–2010 dataset is sorted by AI, from little to high polluted atmosphere, by step of 0.1. Colors represent different aerosol index intervals (mean AI values are reported in figure).The error bars indicate the statistical uncertainties as in Fig. 5.

ACPD
12, 14197–14246, 2012

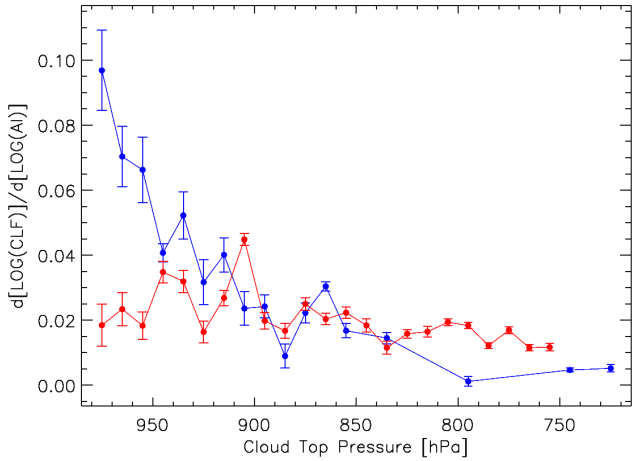

Fig. 10. Cloud fraction sensitivity to aerosol increase (i.e. the computed linear regression slope of CLF-AI relationship in log-log scale) as a function of Cloud Top Pressure (CTP), for cases of mixed (red) and well separated (blue) cloud-aerosol layers, in the region within [4° N, 30° S; 14° W, 18° E]. Dataset is sorted by CTP, from low to high clouds, by step of 10 hPa. The error bars indicate the statistical uncertainties as in Fig. 5.

ACPD
12, 14197–14246, 2012

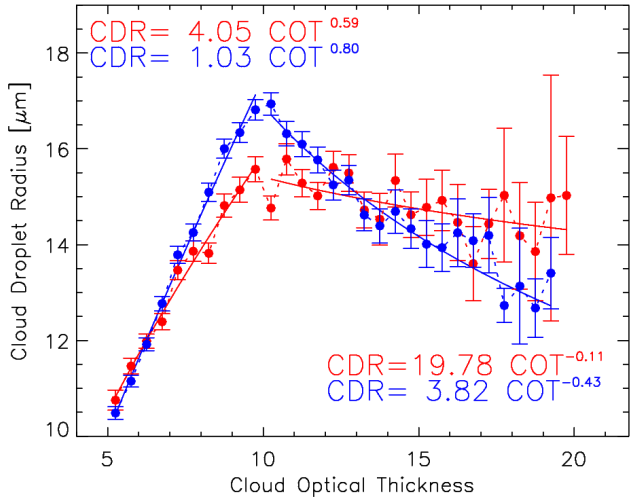

Fig. 11. Cloud Droplet effective Radius (CDR) retrievals averaged over constant bin of Cloud Optical Thickness (COT), for cases of mixed (red) and well separated (blue) cloud-aerosol layers, in the region within [4° N, 30° S; 14° W, 18° E]. In case of mixed layers, only retrievals with AI >0.09 have been selected (polluted clouds). The error bars indicate the statistical uncertainties as in Fig. 5.

ACPD
12, 14197–14246, 2012

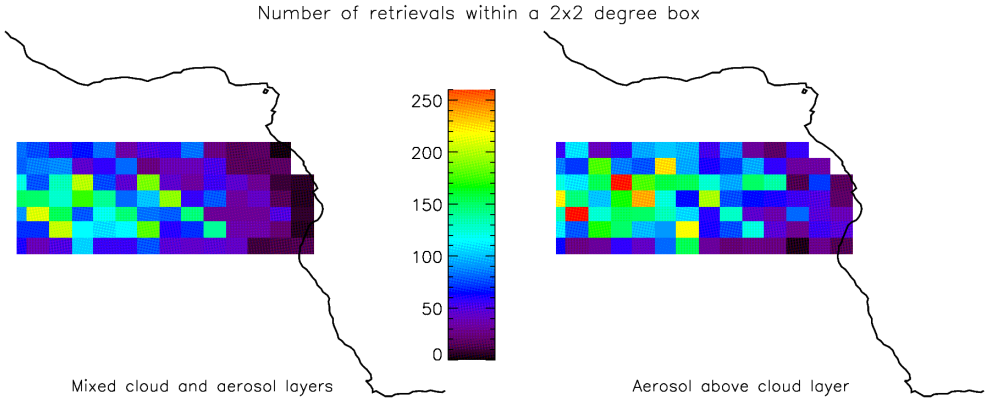

Fig. 12. Number concentration of coincident MODIS-CALIPSO retrievals for all aerosol regimes, in the region within [2° S, 15° S; 14° W, 18° E]. Color scale represents number of measurements within a 2×2 degree box, for cases of mixed (left image) and well separated (right image) cloud-aerosol layers.

ACPD
12, 14197–14246, 2012